IJMMM International Journal of Minerals, Metallurgy and Materials 矿物冶金与材料学报（英文版）

Preparation of sodium molybdate from molybdenum concentrate by microwave roasting and alkali leaching

Fengjuan Zhang, Chenhui Liu, Srinivasakannan Chandrasekar, Yingwei Li, and Fuchang Xu

Cite this article as:
Fengjuan Zhang, Chenhui Liu, Srinivasakannan Chandrasekar, Yingwei Li, and Fuchang Xu, Preparation of sodium molybdate from molybdenum concentrate by microwave roasting and alkali leaching, *Int. J. Miner. Metall. Mater.*, 31(2024), No. 1, pp. 91-105. https://doi.org/10.1007/s12613-023-2727-1

INTERNATIONAL JOURNAL OF
Minerals, Metallurgy and Materials

Volume 31, Number 1, January 2024
Page 91

Research Article https://doi.org/10.1007/s12613-023-2727-1

Preparation of sodium molybdate from molybdenum concentrate by microwave roasting and alkali leaching

Fengjuan Zhang[1)], *Chenhui Liu*[1),✉], *Srinivasakannan Chandrasekar*[2),✉], *Yingwei Li*[3)], *and Fuchang Xu*[4)]

1) School of Chemistry and Environment, Yunnan Minzu University, Kunming 650500, China
2) Chemical Engineering Department, Khalifa University, Abu Dhabi, UAE
3) Yunnan Zhong Tai Technology Co., Ltd., Kunming 650500, China
4) Yunnan Yongchang Silicon Industry Co., Ltd., Baoshan 678000, China
(Received: 15 March 2023; revised: 24 July 2023; accepted: 16 August 2023)

Abstract: The preparation process of sodium molybdate has the disadvantages of high energy consumption, low thermal efficiency, and high raw material requirement of molybdenum trioxide, in order to realize the green and efficient development of molybdenum concentrate resources, this paper proposes a new process for efficient recovery of molybdenum from molybdenum concentrate and preparation of sodium molybdate by microwave-enhanced roasting and alkali leaching. Thermodynamic analysis indicated the feasibility of oxidation roasting of molybdenum concentrate. The effects of roasting temperature, holding time, and power-to-mass ratio on the oxidation product and leaching product sodium molybdate ($Na_2MoO_4·2H_2O$) were investigated. Under the optimal process conditions: roasting temperature of 700°C, holding time of 110 min, and power-to-mass ratio of 110 W/g, the molybdenum state of existence was converted from MoS_2 to MoO_3. The process of preparing sodium molybdate by alkali leaching of molybdenum calcine was investigated, the optimal leaching conditions include a solution concentration of 2.5 mol/L, a liquid-to-solid ratio of 2 mL/g, a leaching temperature of 60°C, and leaching solution termination at pH 8. The optimum conditions result in a leaching rate of sodium molybdate of 96.24%. Meanwhile, the content of sodium molybdate reaches 94.08wt% after leaching and removing impurities. Iron and aluminum impurities can be effectively separated by adjusting the pH of the leaching solution with sodium carbonate solution. This research avoids the shortcomings of the traditional process and utilizes the advantages of microwave metallurgy to prepare high-quality sodium molybdate, which provides a new idea for the high-value utilization of molybdenum concentrate.

Keywords: molybdenum metallurgy; microwave oxidation roasting; removing impurities; sodium hydroxide leaching

1. Introduction

China has an abundance of molybdenum resources, accounting for more than 40% of global molybdenum production [1]. Molybdenum is widely employed for a variety of applications in petroleum, the chemical industry, medicine, biology, agriculture, electronics, electrical, and other fields [2–7]. Sodium molybdate, a molybdenum derivative, also plays a crucial role in different fields, including corrosion inhibitors and inhibitors for steel [8–11], catalysts for pharmaceuticals [12], sewage treatment agents [13], and the manufacture of dyes, inks, and fertilizers. With rising demand for sodium molybdate in a variety of industries, domestic production could exceed 4000 tons per year. The domestic production of sodium molybdate is currently mature. However, the process route encounters the following issues: environmental unfriendliness, serious pollution, and quality failure to meet market demand. The international production process utilizes mostly pure molybdenum trioxide or industrial-grade molybdenum trioxide as the major raw material. Thus, exploring and optimizing the production process and conditions of sodium molybdate is necessary to improve the recovery rate of molybdenum, the purity of sodium molybdate, and environmental benignity.

The current manufacturing technologies of sodium molybdate include the ammonium molybdate liquid alkali method, the molybdenum oxide soda method, the roasted liquid alkali method, the soda nitrate sintering method, the alkali wet method, the acid wet method, and the soda pressurized leaching method. Alkali and acid wet methods require strong oxidants and acids, respectively, which release toxic gases; thus, dealing with toxic gases will raise the cost. The soda ash pressurized leaching method has high requirements for autoclave equipment. Ammonium molybdate liquid alkali and molybdenum oxide soda ash processes are most commonly practiced due to their simplicity and ease of operation. However, the raw materials are ammonium molybdate and molybdenum trioxide. This process has strict requirements on raw materials and high costs. The roasting liquid alkali

✉ Corresponding authors: Chenhui Liu E-mail: liu-chenhui@hotmail.com;
Srinivasakannan Chandrasekar E-mail: srinivasa.chandrasekar@ku.ac.ae

method utilizes molybdenum concentrate and sodium hydroxide as raw materials. First, the molybdenum concentrate is oxidized and roasted to obtain molybdenum calcine and molybdenum trioxide crystals. The molybdenum trioxide is then dissolved in a sodium hydroxide solution to form sodium molybdate after the removal of impurities, filtration, and evaporation crystallization. Rotary cellars [14] and multiple hearth furnaces [15–16] are the traditional roasting equipment for the oxidation roasting of molybdenum concentrate. The rotary cellar is a continuously rotating reactor that facilitates rapid and uniform heating of the material, successfully eliminating sulfur. Multiple hearth furnaces offer superior interfacial contact, thereby facilitating the completion of the oxidation reaction. However, these roasting methods are incompatible with the development policy of green environmental protection, energy savings, and emission reduction. By contrast, as a new heating method, microwave offers fast and uniform heating of the material and is consistent with the concept of green environmental protection.

"Carbon neutrality" has become a popular topic in society in recent years, which requires innovation in energy savings and emission reduction. Metallurgical industries must be innovative to respond to "carbon neutrality." In microwave heating, the microwave energy is absorbed by the material. This phenomenon facilitates the collision of polar molecules within the material with the microwave electromagnetic field, thus converting microwave energy into heat energy and transferring the heat energy directionally to the molecular or atomic reaction through the dielectric consumption of the material itself [17]. Compared with the conventional heating method, microwave heating is characterized by its fast heating speed [18–19] and uniform heating. Without any intermediary medium conduction, the material can be heated by the high-frequency vibration of atoms or molecules in the material under the action of microwave radiation, which further boosts the heating rate. The microwave heating material was evenly heated. The traditional heating method heats from the outside to the inside, resulting in a temperature gradient within the material and uneven heating. Microwave heating generates friction between nearby molecules through high-frequency vibration of the material's internal molecules, heating it from outside to the inside; therefore, the material is heated evenly, and the reaction is adequate [20–21]. Traditional heating generates industrial waste, soot, and toxic gases, thereby polluting the environment, whereas microwave heating is green and environmentally friendly. As a new heating method, microwaves are widely used in metallurgy [22–24]. Zhu *et al.* [25] proposed using microwave sintering of ferronickel slag to prepare insulating materials. They found that microwave heating was beneficial to the formation of magnesium iron chromate and magnesium iron aluminate spinel. Furthermore, compared to conventional sintering, microwave sintering could significantly reduce the sintering temperature and shorten the sintering duration. This study provided a new method for the clean recycling of solid waste resources. Parhi and Misra [26–27] explored a variety of methods to recover molybdenum from waste catalysts. One of these methods entailed using microwave-assisted dilute sulfuric acid leaching to recover molybdenum from spent catalysts to produce molybdenum trioxide. They reported a significant increase in heating rate as well as an increase in molybdenum recovery from 53.35% to over 99% via microwave heating, facilitating the production of high-purity molybdenum trioxide. The study showed the advantages of microwave applications in the field of hydrometallurgy by demonstrating the rising use of microwaves for leaching.

As an important intermediate product in the preparation of sodium molybdate, molybdenum trioxide plays an important part in the recovery of molybdenum. Kan *et al.* [28] investigated the effect of different roasting equipment (chamber furnace, rotary kiln) on the production of molybdenum trioxide from molybdenum concentrate. The sulfur content of the upper and lower parts of the roasting product in the chamber furnace at a large sample height was 1.19% and 7.27%, respectively, rendering it unsuitable for commercial molybdenum trioxide production. In the rotary kiln, it was possible to prepare molybdenum trioxide with a sulfur content of 0.61% by enabling the material to be in uniform and sufficient contact with air. Roasting molybdenum concentrate in box-type furnaces produces a considerable amount of sulfur dioxide, which is difficult to recover and treat, making it environmentally hazardous. The disadvantages of the rotary kiln are slow heating, high power consumption, and uneven temperatures in the furnace. By contrast, the rotary kiln produces substantially higher-quality molybdenum trioxide than the box furnace. However, generating large amounts of dust and polluting the environment is easy during the working process. By contrast, microwave heating can circumvent all the disadvantages due to its green, environmentally friendly, and energy-efficient properties. Microwave roasting of molybdenum concentrate can improve the molybdenum volatilization rate and the product quality due to the superior microwave absorption properties of the molybdenum concentrate. Jiang *et al.* [29] explored the microwave absorption properties of molybdenum concentrate through dielectric properties using the cavity perturbation method. Roasting experiments yielded high-purity α-MoO_3 in a microwave field at 800°C, proving the feasibility of microwave roasting molybdenum concentrate. Pervaiz *et al.* [30] studied the microwave-assisted extraction of molybdenum from molybdenum concentrate to produce ammonium molybdate. First, the molybdenum concentrate is microwave-roasted by mixing with a sodium agent. The molybdenum was extracted in the form of sodium molybdate after roasting, and a crude sodium molybdate solution was produced by water leaching. Calcium molybdate was then obtained by removing impurities and adding calcium chloride. Dried calcium molybdate was refluxed with ammonia for 2 h to obtain ammonium molybdate. This method yielded 31.2% molybdenum with an extraction rate of 83%. Zhang *et al.* [31] explored a new process for the extraction of molybdenum from molybdenum concentrate by microwave roasting and the subsequent preparation of ammonium molybdate. Compared with conventional roasting, microwave roasting of molybdenum concentrate yields ammonium molybdate of high-purity and superior quality.

This study attempts to harness the high efficiency and environmental friendliness of microwave roasting for molybdenum concentrate roasting. This experiment proposes a short, simple, and low-cost method for extracting molybdenum from molybdenum concentrate by microwave roasting and preparing sodium molybdate. Under the influence of microwave roasting, the molybdenum concentrate was utilized as a raw material to prepare high-purity molybdenum trioxide. After alkali leaching and purification, the molybdenum trioxide was then converted to sodium molybdate for high molybdenum recovery. Compared with the traditional method, this method has the advantages of a short process flow and environmental protection, and the SO_2 produced during the roasting process can be directly purified, rendering it clean and environmentally benign.

2. Experimental

2.1. Materials

The molybdenum concentrate used in this experiment was received from Jinduicheng, China, and all reagents used were of analytical grade and contained sodium hydroxide (≥96%, AR) and sodium carbonate (≥99.8%, AR). The aqueous solutions used in the experiments were all deionized water, which was prepared by a laboratory water purification system (Mediu-1600).

2.2. Preparation of sodium molybdate

The method is divided into three major steps: microwave oxidation roasting of molybdenum concentrate, sodium hydroxide leaching, and impurity removal by adjusting the solution termination pH.

2.2.1. Microwave oxidation roasting of molybdenum concentrate

Microwave oxidation roasting of molybdenum concentrate was conducted in a microwave tube furnace. A total of 20 g of molybdenum concentrate was accurately weighed, naturally and evenly distributed on the inner wall of a quartz boat (120 mm × 45 mm × 22 mm) and then placed in the tubular microwave oven for oxidation roasting with air as the oxidant. The target roasting temperature, roasting time, and roasting power were then set. The samples were ground for 3 min after completion of microwave oxidation roasting to achieve uniform mixing of molybdenum calcine. This process produces sulfur dioxide, which is treated by absorption with a sodium hydroxide solution.

2.2.2. Sodium hydroxide leaching

A total of 10 g of molybdenum calcine was combined with 20 mL of 2.5 mol/L NaOH solution in a beaker at a liquid-to-solid ratio of 2 mL/g. The beaker was then placed in a constant temperature water bath at 60°C, sealed, and agitated with a magnetic stirrer for 60 min before leaching. Solid–liquid separation was performed after leaching, and the separated filtrate was used for subsequent experiments.

A 0.5 mol/L Na_2CO_3 solution was added to the filtrate to modify the termination pH of the solution. Na_2CO_3 solution was added drop by drop during the adjustment process and the pH of solution was determined using a pH meter (pHS-3E, Leici, China) until a pH of 8.

After the completion of the pH adjustment, the mixture was placed in a collector-type constant temperature heating magnetic stirrer (DF-101S, Henan Yuhua, China) at 80°C and stirred for 20 min. The mixture was left to stand until the top liquid became clear and transparent. Following the completion of precipitation, the solution was filtered with a circulating water vacuum pump (SHZ-D(Ⅲ), Gongyi Yuhua, China) to remove the impurities. The resulting filtrate was distilled by a rotary evaporator (RE-52AA, Shanghai Yarong, China) to obtain $Na_2MoO_4{\cdot}2H_2O$.

2.3. Characteristic

The chemical composition and elemental content of the samples were analyzed using X-ray fluorescence spectrometry (XRF, EDX-800 ROHS-ASSY, Shimadzu Corporation, Japan). The phase compositions of the molybdenum concentrate, molybdenum calcine, and leach samples were determined using an X-ray diffractometer (Bruker D8 ADVANCE A25X, German). Scanning electron microscopy (SEM, NOVA NANOSEM-450, FEI, USA) equipped with an energy dispersive spectrometer (Octane Pro, USA) was used to examine the materials for microscopic morphology, elemental composition, and distribution. Fourier transform infrared spectroscopy (FTIR, NICOLET IS10 Thermo Fisher Scientific, USA) was used to analyze the structure of functional groups and bond vibrations in the samples. The elemental valence states in the samples were identified using X-ray electron spectroscopy (XPS, Thermo K-Alpha, Thermo Fisher Scientific, USA). The elemental content of the samples was determined using an inductively coupled plasma emission spectrometer (ICP-OES, Agilent ICP-OES 730, USA).

3. Results and discussion

3.1. Analysis of raw material

3.1.1. Experimental material

The molybdenum concentrate used in this study was analyzed by X-ray fluorescence spectroscopy (XRF) for its chemical composition and the content of each element. As shown in Fig. 1(a), the main elements in the molybdenum concentrate were Mo, S, Fe, Si, Al, Cu, and Ca, with the mass percentage of Mo element being 62.17wt%. The XRD physical phase analysis of the molybdenum concentrate is shown in Fig. 1(b). The analysis shows that the element Mo in the molybdenum concentrate exists in the forms of MoS_2 and MoO_3, and the main form is MoS_2, which is accompanied by a small amount of SiO_2 impurities.

Fig. 1(c) and (d) shows the SEM analysis results of the molybdenum concentrate. The results indicate that the molybdenum concentrate has an overall morphology of irregularly shaped and unevenly sized lumps. Holes and cracks were observed on the ore surface, which are conducive to the oxidation reaction. Fig. 1(e) shows the EDS characterization

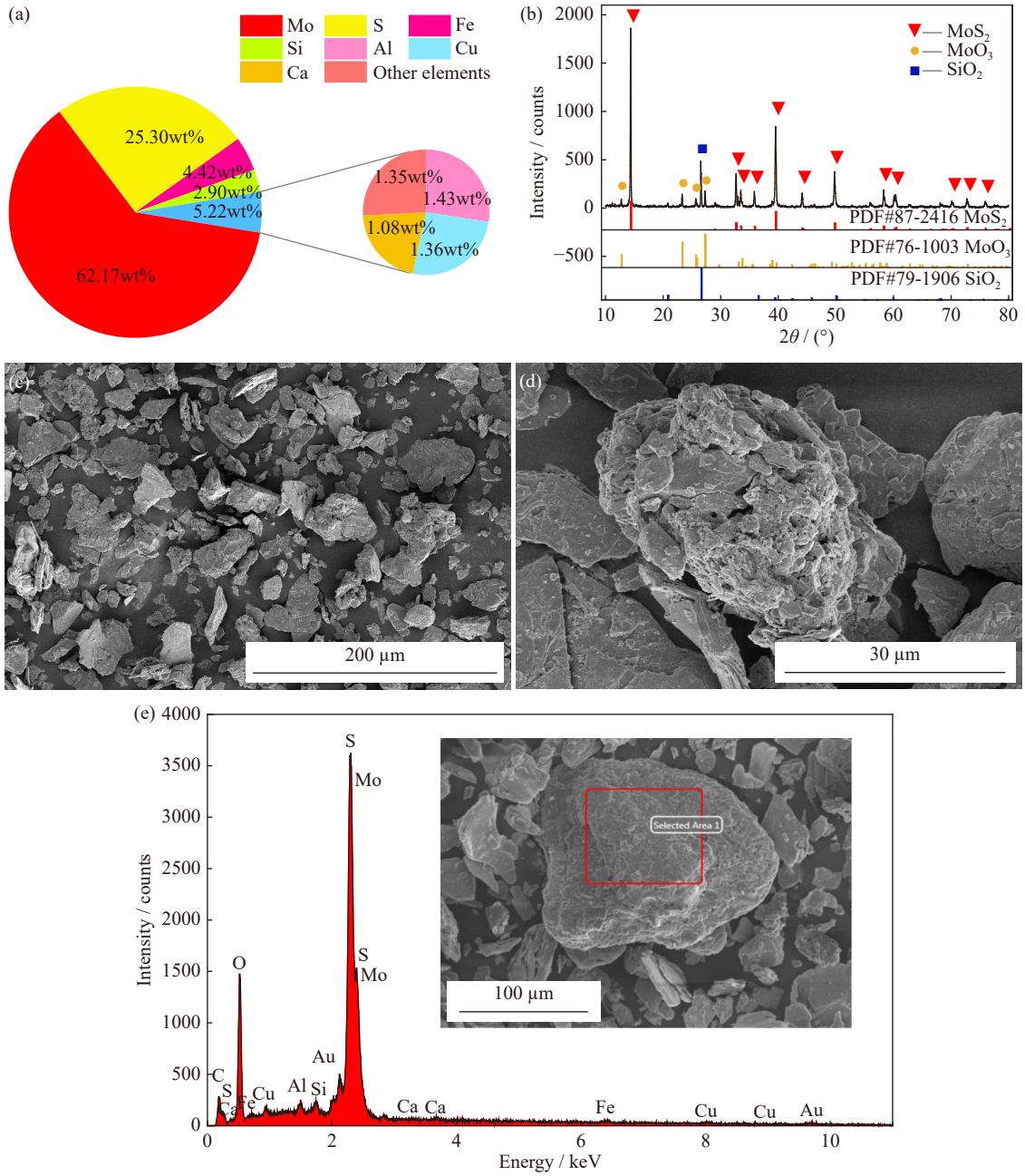

Fig. 1. Molybdenum concentrate characterization: (a) XRF analysis; (b) XRD map; (c–e) SEM–EDS images.

results of the molybdenum concentrate. When combined with the XRD (Fig. 1(b)) analysis, the results show that MoS_2 is the primary component of the molybdenum concentrate, with SiO_2 and other minerals, including elements of Fe, Si, Al, Cu, and Ca as impurities.

3.1.2. Analysis of thermodynamic characteristics

Temperature is a crucial factor in thermodynamics. Analyzing the thermodynamic properties of the oxidation roasting of molybdenum concentrate can provide a theoretical basis because temperature directly affects the quality of the oxidation roast. Therefore, examining the standard Gibbs free energy of the reaction and the dominant interval of each substance is essential.

Table 1 shows the main chemical reactions of oxidation roasting of molybdenum concentrate. The standard Gibbs free energy for each reaction of oxidation roasting in the temperature range of 0–1000°C is negative [31–32], indicating that oxidation roasting is thermodynamically feasible under standard conditions. The oxidation roasting of molybdenum concentrate mainly proceeds with the equation (1). Fig. 2(a) shows that the standard Gibbs free energy of reaction (1) is less than that of reactions (2), (4), (6), and (7) but larger than that of reactions (3), (5), and (8). This finding supports the theory that reaction (1) reacts more than reactions (2), (4), (6), and (7). When the roasting environment is low in oxygen, reactions (3) and (5) tends to occur more than reaction (1). Therefore, adequate oxygen should be maintained during the oxidation roasting process to ensure the occurrence of reaction (1) and inhibit the occurrence of reactions (3) and (5). The temperature required for the oxidation of MoS_2 is

Table 1. Main chemical reaction equations for the oxidation roasting of molybdenum concentrate

No.	Reaction
(1)	$MoS_2 + 3.5O_2(g) = MoO_3 + 2SO_2(g)$
(2)	$MoS_2 + 3O_2(g) = MoO_2 + 2SO_2(g)$
(3)	$MoS_2 + 6MoO_3(g) = 7MoO_2 + 2SO_2(g)$
(4)	$MoO_2 + 0.5O_2(g) = MoO_3$
(5)	$MoS_2 + 27MoO_3(g) = 7Mo_4O_{11} + 2SO_2(g)$
(6)	$Mo_4O_{11} + 0.5O_2(g) = 4MoO_3$
(7)	$2MoS_2 + O_2(g) = Mo_2S_3 + SO_2(g)$
(8)	$Mo_2S_3 + 5O_2(g) = 2MoO_2 + 3SO_2(g)$

reached when the temperature exceeds 500°C, and the oxidation decomposition of the molybdenum concentrate occurs [18]. MoO_3 has a melting point of 795°C. Thus, the oxidation roasting range for this experiment was 550–750°C to achieve as much Mo content in the molybdenum calcine as possible.

Fig. 2(b)–(f) shows the regional dominance diagram of the Mo–O–S system at 550–750°C. The software HSC 6.0 was used to generate the zone dominance plot. The graph reveals that the area of stability interval of MoO_3 increases and then decreases with increasing temperature at fixed oxygen partial pressure $P(O_2)$ and sulfur dioxide partial pressure $P(SO_2)$. By contrast, the amount of oxygen required for the oxidation of MoS_2 to produce MoO_3 gradually increases with rising temperature. The required partial pressure of oxygen is only approximately $1.01 \times 10^{-10.5}$ kPa at a temperature of 550°C and increases to approximately $1.01 \times 10^{-6.5}$ kPa at a temperature of 750°C. Moreover, increasing the temperature is favorable to the formation of MoO_3 based on the change in the stable interval region of MoS_2, and adequate oxygen is required to maximize the conversion of MoS_2 to MoO_3.

3.2. Effect of oxidation roasting on the preparation of $Na_2MoO_4 \cdot 2H_2O$ by alkali leaching

3.2.1. Influence of roasting temperature

Experiments were conducted at temperatures ranging from 550 to 750°C to examine the effect of different roasting temperatures on the preparation of $Na_2MoO_4 \cdot 2H_2O$. The molybdenum calcine was leached at room temperature for 60 min using 2.5 mol/L sodium hydroxide in a liquid-to-solid ratio of 2 mL/g.

Fig. 3(a) shows that the roasting temperature has a strong influence on the crystallization ratio of MoO_3 and the Mo content in the molybdenum calcine. The crystallization ratio of MoO_3 and the Mo content in the molybdenum calcine increased with the increase of temperature from 550 to 750°C. This trend can be attributed to the increase in MoO_3 vapor pressure with rising temperatures [33], breaking the oxide film and volatilizing MoO_3. The volatilized MoO_3 exits the primary heat source and enters the nucleation zone, where it condenses and crystallizes at a maximum crystallization ratio at 700°C. Simultaneously, with an increase in temperature, the reaction rate would increase the conversion of additional MoS_2, raising the Mo content in the molybdenum calcine. At 750°C, owing to the high localized temperature, the sintering of molybdenum concentrate at the bottom limits the diffusion of oxygen inside the sample, resulting in insufficient oxidation roasting and a reduction in the Mo content of the molybdenum calcine [34]. By contrast, when the roasting temperature was 750°C, fewer MoO_3 needle-like crystals were observed in the center of the roasted product because crystal formation starts when MoO_3 leaves the molybdenum concentrate. As MoO_3 leaves the heat source, it will condense into MoO_3 crystals at the nucleation position due to the low temperature [33]. When the temperature is too high, the temperature at the nucleation position of MoO_3 may not real-

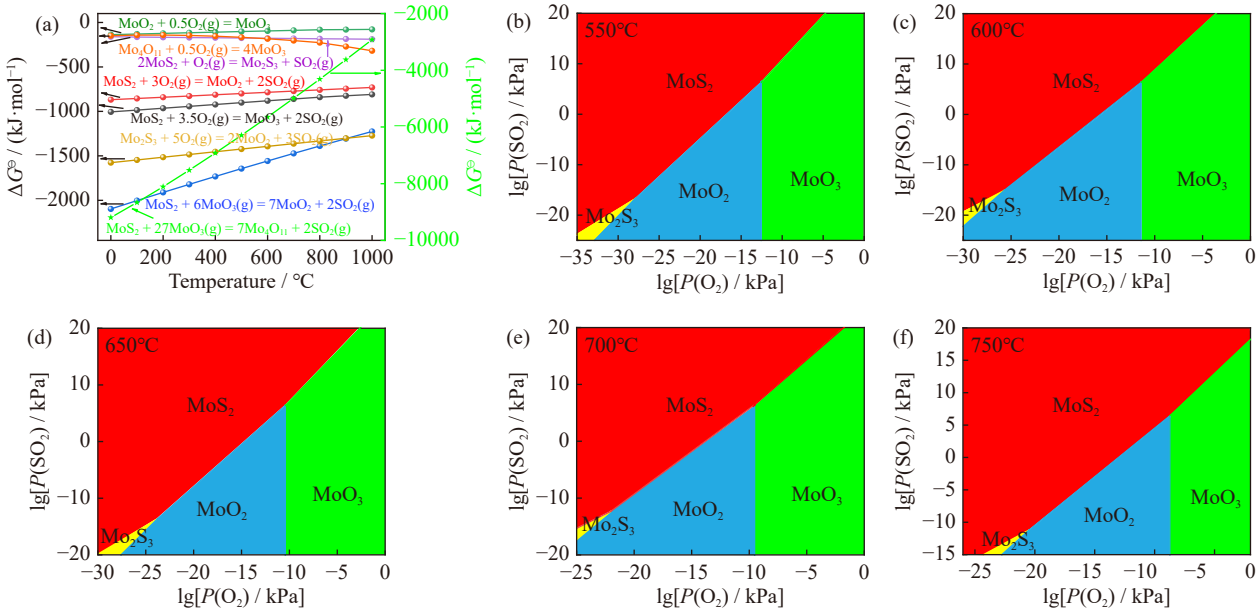

Fig. 2. (a) $\Delta G^{\ominus}$ versus temperature for the main chemical equations in the oxidation roasting of molybdenum concentrate; (b–f) map of the areas of advantage of the Mo–O–S system at different temperatures.

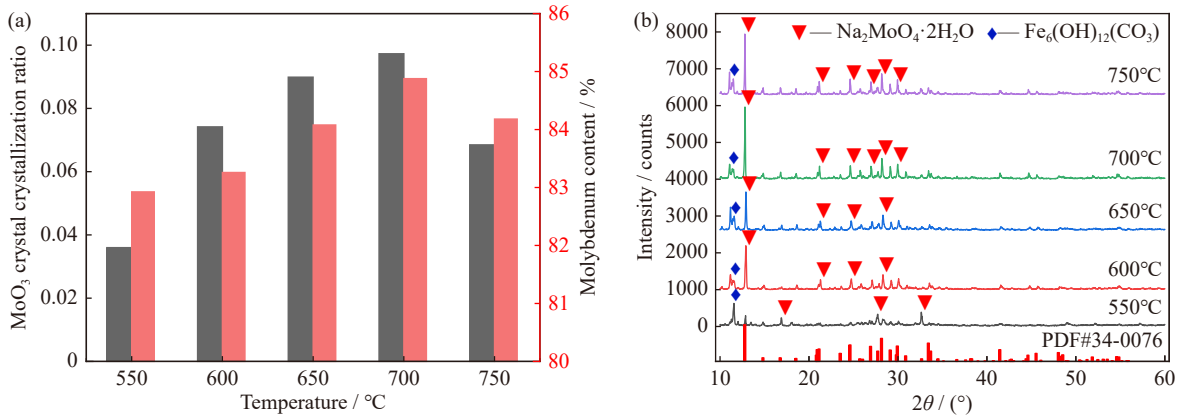

Fig. 3. Effect of roasting temperature on molybdenum calcine and $Na_2MoO_4·2H_2O$: (a) MoO_3 crystal crystallization ratio and molybdenum content in the molybdenum calcine; (b) XRD spectra of $Na_2MoO_4·2H_2O$.

ize the condensation condition, resulting in a slow MoO_3 crystallization ratio.

Fig. 3(b) shows the XRD spectrum of $Na_2MoO_4·2H_2O$, which demonstrates that the peak of $Na_2MoO_4·2H_2O$ gradually intensifies from 550 to 700°C. This observation is due to the higher MoO_2 content in molybdenum calcine at low roasting temperatures than at high roasting temperatures, with the highest MoO_3 content at 700°C. When combined with Fig. 3(a), the oxidation reaction of molybdenum concentrate at a roasting temperature of 700°C is highly adequate. The tendency for NaOH alkali leaching improves when the MoO_3 content is high [35]. The amount of MoO_3 in molybdenum calcine reduces at 750°C due to insufficient oxidation roasting, which resulted in poor NaOH leaching. Therefore, the diffraction peak of $Na_2MoO_4·2H_2O$ slightly weakens. The optimal oxidation roasting temperature was determined to be 700°C based on the analysis.

3.2.2. Influence of holding time

Different holding time have a substantial effect on the preparation of $Na_2MoO_4·2H_2O$. The effect of different holding time ranging from 30 to 130 min on the formation of $Na_2MoO_4·2H_2O$ was investigated by controlling the roasting temperature of 700°C and the power-to-mass ratio of 110 W/g.

As shown in Fig. 4(a), the crystallization ratio of MoO_3 and the Mo content in the molybdenum calcine steadily rise with the holding time increasing until the ideal duration of 110 min. Due to the excessively short holding time, a large amount of MoS_2 at the bottom of the sample does not react completely. With the increase of holding time, enough oxygen gradually enters the bottom of the sample, the MoS_2 is fully oxidized. The content of MoO_3 was high at a holding time of 110 min. The production of MoO_2 in the sample may open the structures, increasing the rate of MoO_3 volatilization and crystallization in the nucleation sites. Therefore, the crystallization ratio of MoO_3 and the Mo content in the molybdenum calcine increased with the rising of holding time, peaking at 110 min. The escaping of MoO_3 vapor through the cracks is responsible for the reduction in crystallization ratio and Mo content at temperatures above 110°C.

Fig. 4(b) shows that XRD diffraction peaks of $Na_2MoO_4·2H_2O$ increase and strengthen with the increase in holding time from 30 to 110 min. This phenomenon could be attributed to the inadequate oxygen in the air, and MoS_2 will react with O_2 and MoO_3 to generate the intermediate product MoO_2 [33]. As the holding time increases, MoO_2 will further react with O_2 to generate MoO_3. However, alkali leaching prefers the presence of MoO_3 over MoO_2. NaOH preferentially leaches MoO_3 when MoO_3 and MoO_2 are present in the molybdenum calcine. The leaching efficiency of NaOH is low when the MoO_2 content is high [35]. The XRD diffraction peaks of $Na_2MoO_4·2H_2O$ weaken when the holding time

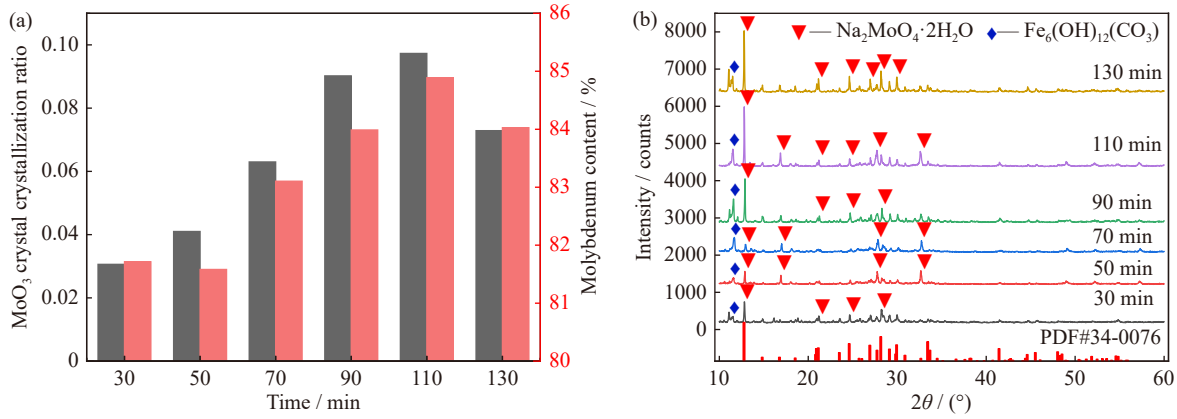

Fig. 4. Effect of holding time on molybdenum calcine and $Na_2MoO_4·2H_2O$: (a) MoO_3 crystal crystallization ratio and Molybdenum content in the molybdenum calcine; (b) XRD spectra of $Na_2MoO_4·2H_2O$.

increases to 130 min. Therefore, 110 min was chosen as the optimal holding time.

3.2.3. Influence of power-to-mass ratio

The effect of the power-to-mass ratio was assessed in the range of 70 to 120 W/g to optimize the effect of this ratio on the preparation of $Na_2MoO_4{\cdot}2H_2O$. Fig. 5(a) shows that in the power-to-mass range of 70 to 80 W/g, the crystallization ratio of MoO_3, and the Mo content in molybdenum calcine decrease, which can be attributed to the variance in the experiment. The graph shows that in the range of 80 to 100 W/g, with the microwave power increasing, the crystallization ratio of MoO_3 and the Mo content in the molybdenum calcine generally increase, reaching a maximum at 100 W/g. This trend demonstrates that oxidation roasting is superior when microwave power increases for a given mass. Molybdenum concentrate has strong dielectric properties and can effectively absorb microwave energy. The strength of the electric field increases with microwave power. The absorbed microwave power per unit volume is proportional to the square of the electric field strength. Therefore, the amount of heat generated per unit volume and time will increase. Increased heating encourages oxidation roasting, raising the Mo content and the crystallization ratio of MoO_3. However, exceeding the optimal microwave power will trigger sintering in the product. This phenomenon could be explained by an increase in the heat absorbed by the molybdenum concentrate, which causes local overheating and sintering as well as a reduction in the MoO_3 content, lowering the crystallization ratio of MoO_3 and the Mo content of the molybdenum calcine [36].

Fig. 5(b) shows the XRD diffraction pattern of $Na_2MoO_4{\cdot}2H_2O$ as influenced by different power-to-mass ratios. Combined with the analysis in Fig. 5(a), as the microwave power increases, when the microwave energy passes through the material, the heat generated due to dielectric loss increases, the molybdenum concentrate is fully oxidized and roasted, and a high MoO_3 content is generated by the reaction. Therefore, with the increase in microwave power, the $Na_2MoO_4{\cdot}2H_2O$ XRD peak gradually enhanced, with the highest peak observed at 100 W/g, indicating the presence of the most fully oxidized molybdenum concentrate at this time. The XRD peak of leaching to produce $Na_2MoO_4{\cdot}2H_2O$ weakens as the microwave power continued to increase. Therefore, the optimal power-to-mass ratio is 100 W/g.

3.2.4. Discussion of the effect of oxidation roasting on the preparation of $Na_2MoO_4{\cdot}2H_2O$ by alkali leaching

The experimental analysis shows that the optimum roasting conditions for the microwave oxidation roasting stage are as follows: roasting temperature of 700°C, holding time of 110 min, and power-to-mass ratio of 100 W/g.

Fig. 6 depicts XRD and SEM analyses of the roasted molybdenum calcine. Fig. 6(a) and (b) shows the XRD and EDS analyses of molybdenum calcine, respectively, which prove the complete conversion of MoS_2 to MoO_3. However, a few impurities, such as $Fe_2(MoO_4)_3$, SiO_2, and other impurities containing aluminum elements, are observed in molybdenum calcine [37–38]. The formation of $Fe_2(MoO_4)_3$ may be due to the MoO_3 generated at the bottom of the molybdenum concentrate during roasting due to the excessively thick material layer for crystal formation. Therefore, a small amount of $Fe_2(MoO_4)_3$ is generated by reaction of MoO_3 with iron-containing impurities near the bottom of the material. Fig. 6(c) and (d) shows the SEM morphologies of molybdenum calcine at different magnifications. Fig. 6(c) reveals that molybdenum calcine has a loose and porous structure with several plate-like MoO_3 crystals and flake crystals attached to the surface. The formation of flake crystals may be attributed to the internal release of gaseous SO_2 generated during the reaction of the molybdenum concentrate. The large amount of MoO_3 on the surface of molybdenum calcine, as well as its loose and porous structure, accelerates the reaction with sodium hydroxide solution during the alkali leaching stage [39] and allow sodium hydroxide to penetrate the interior of molybdenum calcine, increasing and promoting contact. The surface scan results in Fig. 6(e)–(j) further demonstrate that the main substance in the roasted product molybdenum calcine is MoO_3, which is uniformly distributed on the surface of the molybdenum calcine. Impurities include $Fe_2(MoO_4)_3$, SiO_2, and aluminum element. The aluminum elements and silicon elements are uniformly dispersed on the surface of the fragments, while the iron elements are scattered sporadically on the edge part of the fragments.

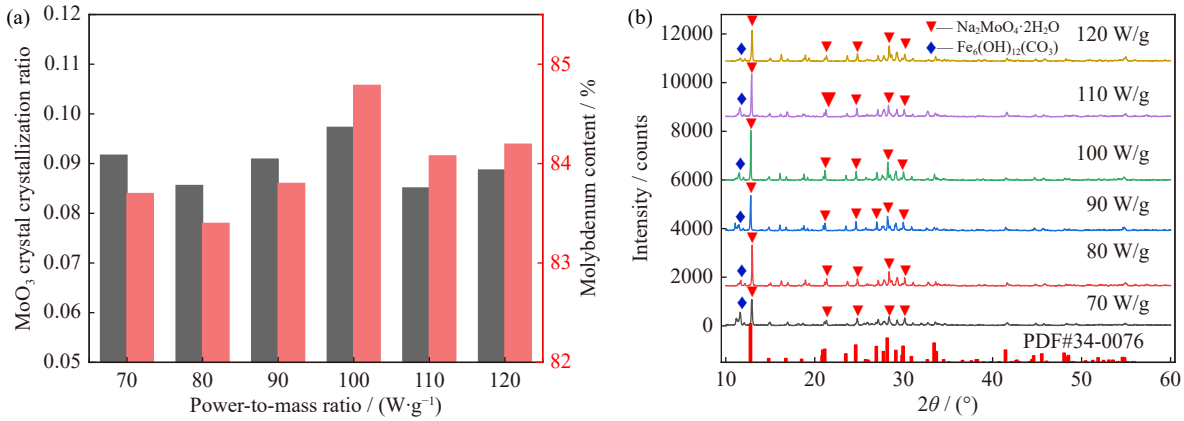

Fig. 5. Effect of power-to-mass ratio on molybdenum calcine and $Na_2MoO_4{\cdot}2H_2O$: (a) MoO_3 crystal crystallization ratio and molybdenum content in the molybdenum calcine; (b) XRD spectra of $Na_2MoO_4{\cdot}2H_2O$.

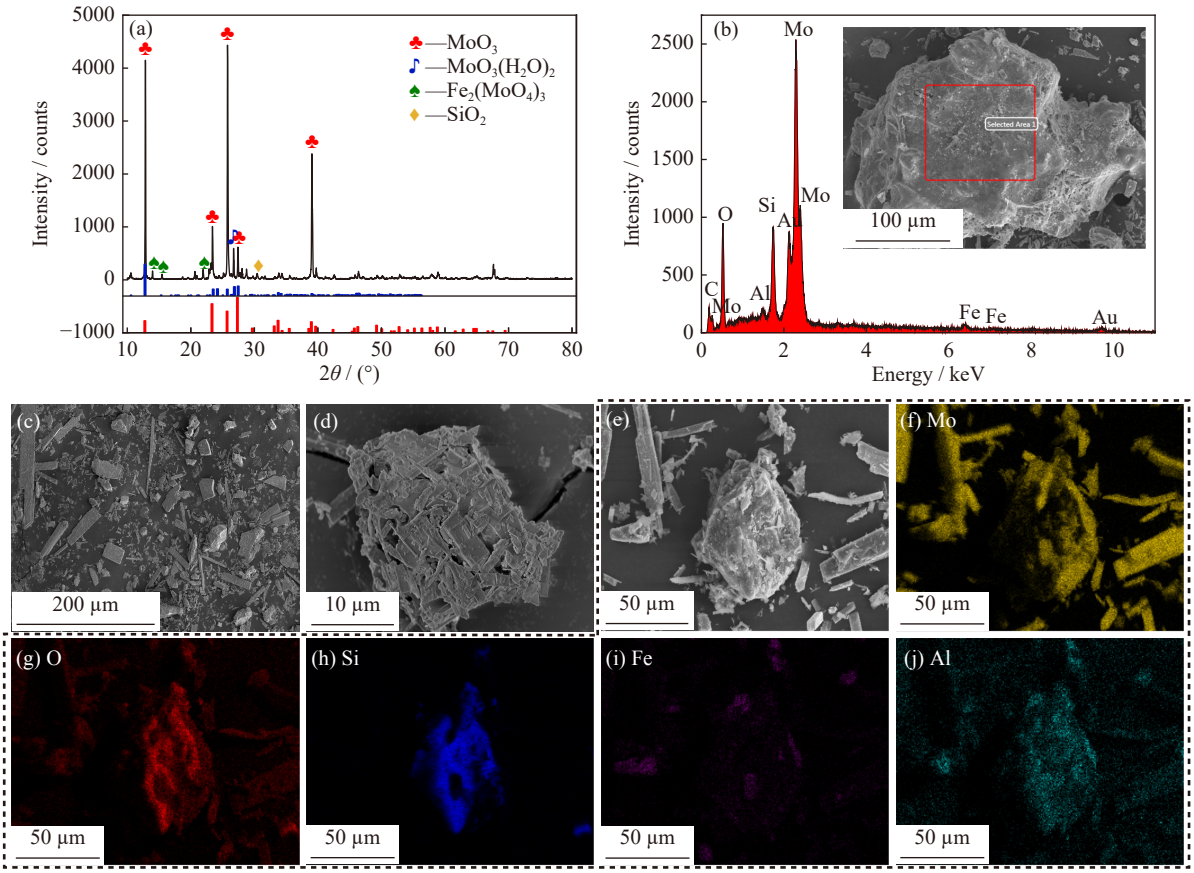

Fig. 6. Characterization of molybdenum calcine: (a) XRD analysis; (b–d) SEM–EDS images of molybdenum calcine; (e–j) surface scan analysis of molybdenum calcine.

3.3. Effect of leaching parameters on the preparation of $Na_2MoO_4·2H_2O$

The leaching of molybdenum calcine using NaOH solution is a typical liquid–solid reaction. Therefore, the leaching solution concentration, liquid-to-solid ratio, and leaching temperature are all key factors influencing the leaching reaction [1]. The alkali leaching experiments were all performed with molybdenum calcine produced at a roasting temperature of 700°C, a holding time of 110 min, and a power-to-mass ratio of 100 W/g as raw material.

3.3.1. Influence of NaOH concentration

The effect of different concentrations of NaOH solution ranged from 2 to 4 mol/L on the leaching of $Na_2MoO_4·2H_2O$, with the other parameters remaining constant at a liquid-to-solid ratio of 2 mL/g, a leaching temperature of 60°C, and a solution termination pH of 9.

In this leaching experiment, NaOH concentration is one of the key factors affecting the leaching experiment [40]. Fig. 7(a) shows that the XRD diffraction peaks of $Na_2MoO_4·2H_2O$ were the highest when the NaOH concentration was 2.5 mol/L. The XRD diffraction peaks of $Na_2MoO_4·2H_2O$ gradually decreased when the NaOH concentration increased from 2.5 to 4 mol/L. This phenomenon is attributed to an increase in reaction rate as well as the mass transfer rate with increasing concentration, which contributes to an increase in Mo recovery, represented in increased $Na_2MoO_4·2H_2O$ [41]. However, as the NaOH concentration continues to increase, the XRD diffraction peaks of $Na_2MoO_4·2H_2O$ weaken and decrease, indicating that the leaching activity of molybdenum decreases at high NaOH concentrations [42]. This finding may also be due to the stoichiometric limitation and the reaction of the high NaOH concentration with other metal impurities in the solution, resulting in a decrease in Mo content.

Fig. 7(b) shows that the highest leaching rate of $Na_2MoO_4·2H_2O$ was 83.1% at a NaOH concentration of 2.5 mol/L. Combined with Fig. 7(a), the optimal NaOH concentration is 2.5 mol/L.

3.3.2. Influence of liquid-to-solid ratio

The effect of a liquid-to-solid ratio ranging from 1 to 4 mL/g on the leaching of $Na_2MoO_4·2H_2O$ was assessed while maintaining the NaOH concentration at 2.5 mol/L, the leaching temperature at 60°C, and the solution termination pH at 9.

The results in Fig. 8(a) show that with the increase in the liquid-to-solid ratio, the XRD diffraction peaks of $Na_2MoO_4·2H_2O$ are the most and strongest at the liquid-to-solid ratio of 2 mL/g, while the diffraction peaks weaken as the liquid-to-solid ratio increases further. This finding is due to the increase in the number of ions reacting with MoO_3 in the system and the large amount of solution surrounding the surface of the solid particles when the liquid-to-solid ratio increases, and the mass transfer area of liquid-solid phases increases, which facilitates the diffusion of the reaction medium and raise the leaching rate of Mo [43–45]. The aforemen-

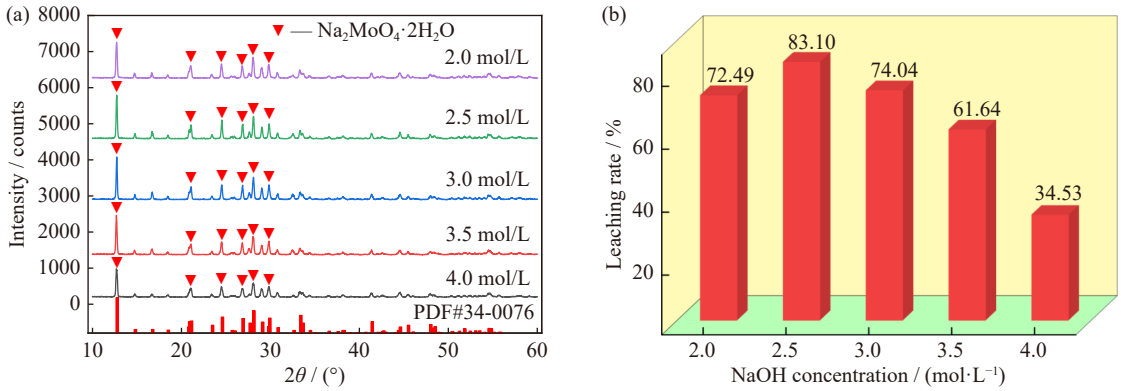

Fig. 7. Effect of sodium hydroxide concentration on the preparation of $Na_2MoO_4·2H_2O$: (a) XRD spectra of $Na_2MoO_4·2H_2O$; (b) sodium molybdate leaching rate.

tioned phenomenon also enhances the penetration of solution into the interior of the solid particles [46–48] and increases the solubility of Mo [35], reaching equilibrium at 2 mL/g, which is enough to dissolve the molybdenum in the molybdenum calcine [49]. The XRD diffraction peaks of $Na_2MoO_4·2H_2O$ tended to decrease with the continuous increase in the liquid-to-solid ratio. Thus, increasing the liquid-to-solid ratio might lead to the leaching of other metal ions from the solution. Excess NaOH will react with other metal ions in the solution, resulting in reduced Mo content.

Fig. 8(b) shows that the leaching rate of $Na_2MoO_4·2H_2O$ increased with the rising of liquid-to-solid ratio from 1 to 2 mL/g. The leaching rate of $Na_2MoO_4·2H_2O$ was the highest at a liquid-to-solid ratio of 2 mL/g, and continuously increasing the liquid-to-solid ratio was unfavorable for the preparation of $Na_2MoO_4·2H_2O$. Combined with Fig. 8(a), the results further demonstrated that the liquid-to-solid ratio of 2 mL/g has the highest leaching efficiency and is the most favorable for the preparation of $Na_2MoO_4·2H_2O$ by leaching. Therefore, the optimal condition for the liquid-to-solid ratio is 2 mL/g.

3.3.3. Influence of leaching temperature

The effects of different leaching temperatures ranging from 20 to 80°C on the leaching of $Na_2MoO_4·2H_2O$ were investigated. The NaOH concentration was 2.5 mol/L, the liquid-to-solid ratio was 2 mL/g, and the solution termination pH was 9.

For chemical reactions, the reaction temperature has a remarkably strong influence on how completely the reaction proceeds, and the reaction is typically expected to proceed fully as the reaction temperature increases [50]. For this experiment, as the leaching temperature increases, the percentage of dissolved solid particles increases, and low temperature conditions may not complete the efficient leaching of molybdenum. Fig. 9(a) shows an increase in the XRD diffraction peak of $Na_2MoO_4·2H_2O$ with an increase in the leaching temperature until 60°C. On the one hand, the reaction equilibrium constant is affected by temperature, which increases with the reaction temperature. Thus, the chemical reaction proceeds forward, and the solubility of solid particles increases. On the other hand, high temperatures are conducive to mass transfer [51], and more molecules in solutions with higher translational energy than activation energy prompt an increase in reaction rate. The decrease of diffraction peak of $Na_2MoO_4·2H_2O$ at 80°C could be attributed to the substitution reaction of OH^- in NaOH solution to produce alcohol and acid due to the high temperature.

Fig. 9(b) further demonstrates that with an increase in leaching temperature, the reaction between NaOH solution and MoO_3 can be promoted. Consequently, the leaching rate of $Na_2MoO_4·2H_2O$ increases and reaches its maximum value at 60°C. Therefore, the optimal leaching temperature is 60°C.

3.3.4. Influence of solution pH

In this experiment, adjusting the solution termination pH

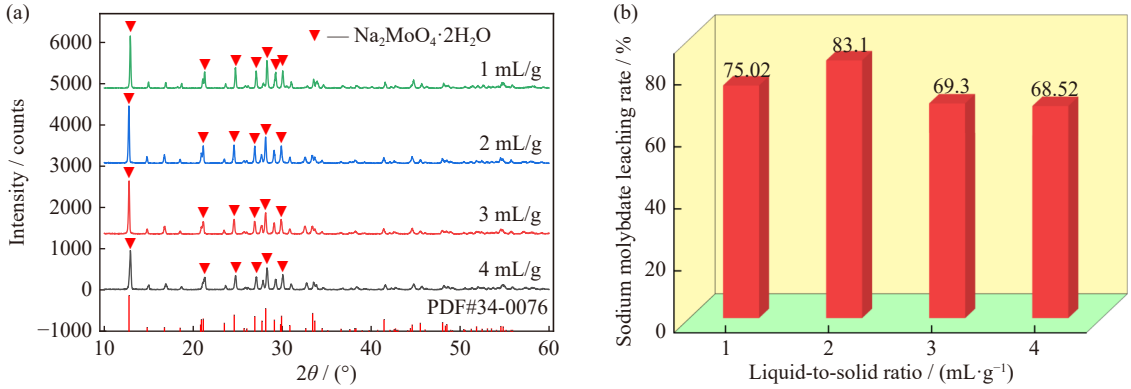

Fig. 8. Effect of liquid-to-solid ratio on the preparation of $Na_2MoO_4·2H_2O$: (a) XRD spectra of $Na_2MoO_4·2H_2O$; (b) sodium molybdate leaching rate.

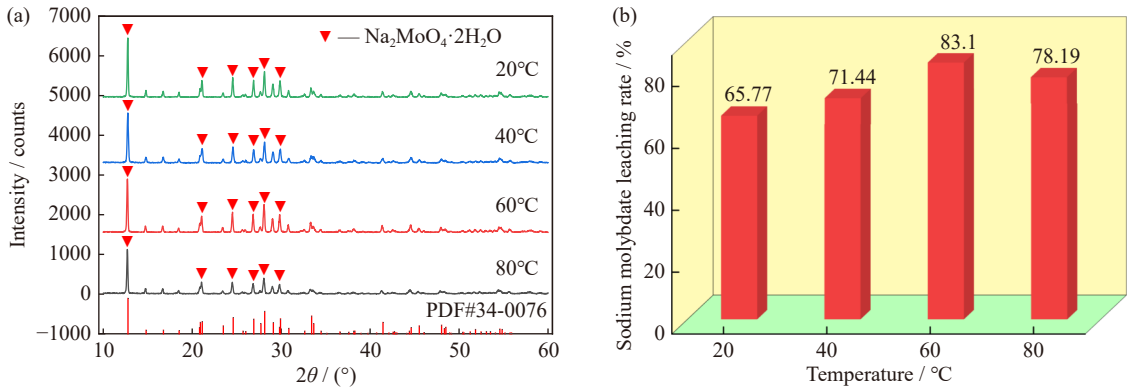

Fig. 9. Effect of leaching temperature on the preparation of $Na_2MoO_4·2H_2O$: (a) XRD spectra of $Na_2MoO_4·2H_2O$; (b) sodium molybdate leaching rate.

is a crucial step for the preparation of $Na_2MoO_4·2H_2O$. The effects of different solution pH ranging from 8 to 11 on the leaching of $Na_2MoO_4·2H_2O$ were assessed, with the other parameters remaining at the NaOH concentration of 2.5 mol/L, the liquid-to-solid ratio of 2 mL/g, and the leaching temperature of 60°C.

The pH of the solution affects the leaching of sodium molybdate. The solution contains a significant proportion of iron elements, and the iron element impurities can simply be removed by altering the solution pH to an alkaline condition. The solution also contains some aluminum element impurities. Therefore, Na_2CO_3 was chosen to adjust the solution pH, and the ionic reactions (9) and (10) show the reaction mechanism.

$$2Fe^{3+} + 3CO_3^{2-} + 3H_2O = 2Fe(OH)_3 \downarrow + 3CO_2(g) \quad (9)$$

$$2Al^{3+} + 3CO_3^{2-} + 3H_2O = 2Al(OH)_3 \downarrow + 3CO_2(g) \quad (10)$$

Fig. 10(a) shows impurities in the unpurified $Na_2MoO_4·2H_2O$ under the same experimental conditions. The diffraction peaks of XRD are extremely weak, and many diffraction peaks of $Na_2MoO_4·2H_2O$ do not appear obviously. After adjusting the pH, pure $Na_2MoO_4·2H_2O$ could be obtained, as evidenced by the strong XRD diffraction peaks. With the increase in solution pH, the XRD diffraction peaks of $Na_2MoO_4·2H_2O$ gradually weakened. The XRD diffraction peaks of $Na_2MoO_4·2H_2O$ at pH 8 were the strongest and most numerous.

Fig. 10(b) shows a maximum leaching rate of 96.24% in $Na_2MoO_4·2H_2O$ when the solution termination pH is 8. This finding further proves that the increase in solution pH is not conducive to the purification of $Na_2MoO_4·2H_2O$. This phenomenon may be due to the enhanced leaching of other metal impurities with the increase in solution alkalinity. Therefore, the optimal pH for solution leaching is 8.

3.3.5. Content of sodium molybdate

Under optimal experimental conditions, the mass fraction of molybdenum and sodium elements in the samples was tested by ICP-OES. The content of sodium molybdate was calculated using the following formula:

$$\omega_1 = \omega_2 + \omega_3 + \left(\frac{m \times \omega_2}{M_2} \times 6\right) M_3 + \left(\frac{m \times \omega_2}{M_2} \times 4\right) M_4 \quad (11)$$

where ω_1 is the mass fraction of sodium molybdate, ω_2 is the mass fraction of the molybdenum element, ω_3 is the mass fraction of sodium element, M_2 is the relative atomic mass of the molybdenum element, M_3 is the relative atomic mass of the oxygen element, M_4 is the relative atomic mass of the hydrogen element, and m is the mass of sodium molybdate. Under optimal conditions, the content of sodium molybdate is 94.08wt% from formula (11).

3.4. Characterization

3.4.1. Scanning electron microscope analysis

Fig. 11 shows SEM results of $Na_2MoO_4·2H_2O$. It reveals that $Na_2MoO_4·2H_2O$ is irregularly shaped and unevenly sized with smooth surfaces and loosely packed together to form fragments. The EDS and surface scan results are in accord-

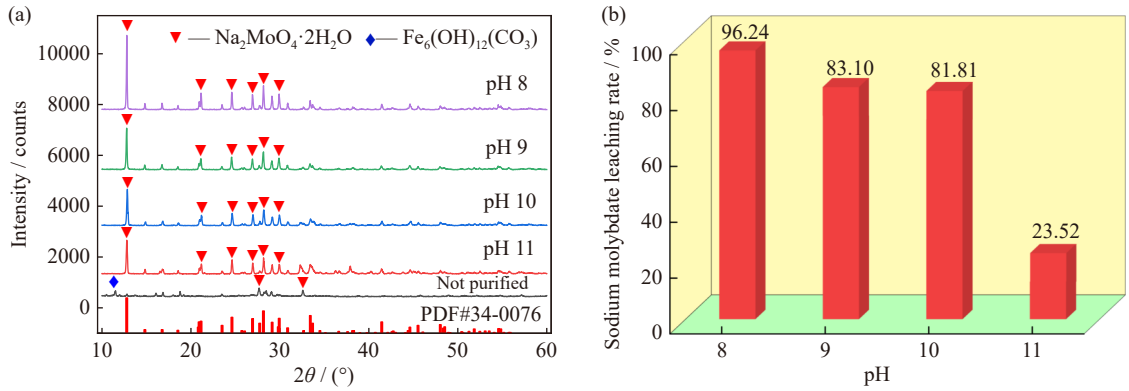

Fig. 10. Effect of solution termination pH on the preparation of $Na_2MoO_4·2H_2O$: (a) XRD spectra of $Na_2MoO_4·2H_2O$; (b) sodium molybdate leaching rate.

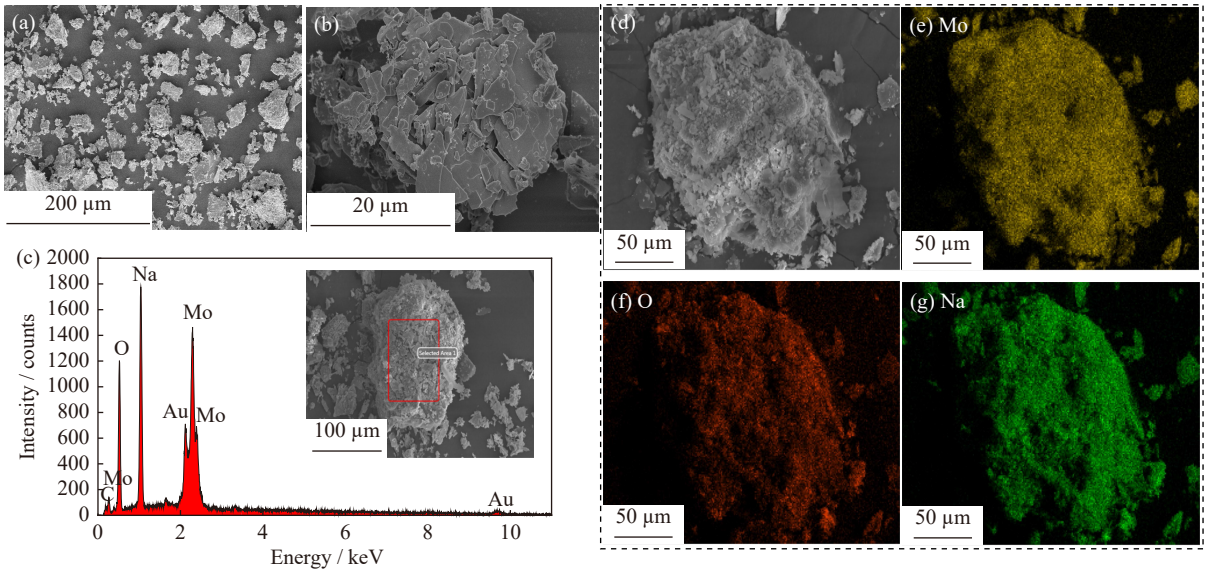

Fig. 11. Characterization of sodium molybdate: (a, b) SEM images; (c) EDS analysis; (d–g) surface scan analysis.

ance with the expectation, containing only Mo, O, and Na, and the elements are densely and uniformly dispersed on the entire fragment surface.

Fig. 12 shows the SEM–EDS analysis results of impure $Na_2MoO_4{\cdot}2H_2O$. Fig. 12(a) reveals that the impure $Na_2MoO_4{\cdot}2H_2O$ is a particle with an uneven and rough surface. The particles are loosely stacked together by flakes and strips of crystals of different sizes. This morphology provides favorable conditions for alkali leaching to remove impurities because the uneven surface can increase the contact area with the Na_2CO_3 solution, favoring enhanced leaching rate. The EDS results shown in Fig. 12(c) indicate that the contained elements are mainly Mo, O, and Na, and the remaining small amounts of Al and Fe elements are impurities. The surface scan results further prove that the unpurified $Na_2MoO_4{\cdot}2H_2O$ is accompanied by impurities of Al and Fe elements. The distribution of elements Mo, O, and Na is uniform and dense, and impurities of Al and Fe elements are also uniformly distributed on the surface of the particles.

Fig. 13 shows the SEM–EDS analysis results of the alkali-leached slag and impurity slag. Fig. 13(a) shows the alkali-leached slag. $Na_2MoO_4{\cdot}2H_2O$ crystals were found on the surface of alkali-leached slag, which was consistent with EDS results. EDS results show that the alkali-leached slag contains many $Na_2MoO_4{\cdot}2H_2O$ and SiO_2, as well as some Fe, Al, Cu, and Ca elements, which are consistent with the results of XRF and EDS (Fig. 1) analyses of the molybdenum concentrate. SEM results show the rough and irregular morphology of alkali-leached slag, suggesting that molybdenum calcine is dissolved during leaching [52]. NaOH solution can remove a large amount of SiO_2 impurities from molybdenum calcine. SiO_2 dissolves in a hot concentrated strong alkali solution, and impurities in SiO_2 can be successfully eliminated by controlling the concentration of NaOH solution and leaching temperature. Elements such as Fe, Al, Cu, and Ca can also form precipitates that remain in the alkali-leached slag during the alkali leaching process.

Fig. 13(b) shows the SEM–EDS analysis of the impurity slag, which has a lumpy structure with a smooth surface and a small amount of $Na_2MoO_4{\cdot}2H_2O$. The EDS results reveal that the impurity slag contains elements Mo, O, Na, Fe, and Al. This finding proves that sodium carbonate can effectively remove impurities such as Fe and Al elements. This phenomenon is due to the reaction with sodium carbonate to form $Fe(OH)_3$ and $Al(OH)_3$ precipitation, which are separated from the $Na_2MoO_4{\cdot}2H_2O$ solution in the form of precipitate and left in the impurity slag.

3.4.2. FTIR analysis

Fig. 14 shows the FTIR spectroscopy results of $Na_2MoO_4{\cdot}2H_2O$ used to determine the molecular structure and chemical composition of the substances. Fig. 14(a) reveals the FTIR spectrum of $Na_2MoO_4{\cdot}2H_2O$. The presence of sodium is demonstrated by the characteristic peak at 1364.66 cm^{-1}. The very strong stretching and weak bending vibrations of Mo–O in MoO_4^{2-} are at 831.81–899.54 and 546.35–642.47 cm^{-1}, respectively. The O–H bond in the water molecules is responsible for the characteristic peak at 3304.73 cm^{-1} in the high wave number region [31,53–54]. Fig. 14(b) shows the FTIR spectrum of impure $Na_2MoO_4{\cdot}2H_2O$, which reveals the presence of the sodium characteristic peak, demonstrating a faint Mo–O bond stretching vibration at 832.18 cm^{-1}. The absence of the impurity Fe characteristic peak in the spectrum is most likely due to its low content. In addition to the characteristic absorption peaks of sodium and Mo–O. Fig. 14(c) shows the FTIR spectrum of alkali-leached slag and the presence of overtone bands of Fe–O at 1067.57 cm^{-1}, where the peaks at 796.53 and 466.55 cm^{-1} are symmetric stretching and bending vibrations of the Si–O bond, respectively. Fig. 14(d) shows the FTIR spectrum of impurity slag, which proves the characteristic absorption peaks of Fe–OH bonds in $Fe(OH)_3$ at 1387.35 and 468.46 cm^{-1} [55]. This finding shows that pH adjustment by sodium carbonate can effectively remove iron impurities.

3.4.3. XPS analysis

XPS techniques were used to investigate the elemental composition and elemental valence of $Na_2MoO_4{\cdot}2H_2O$. The

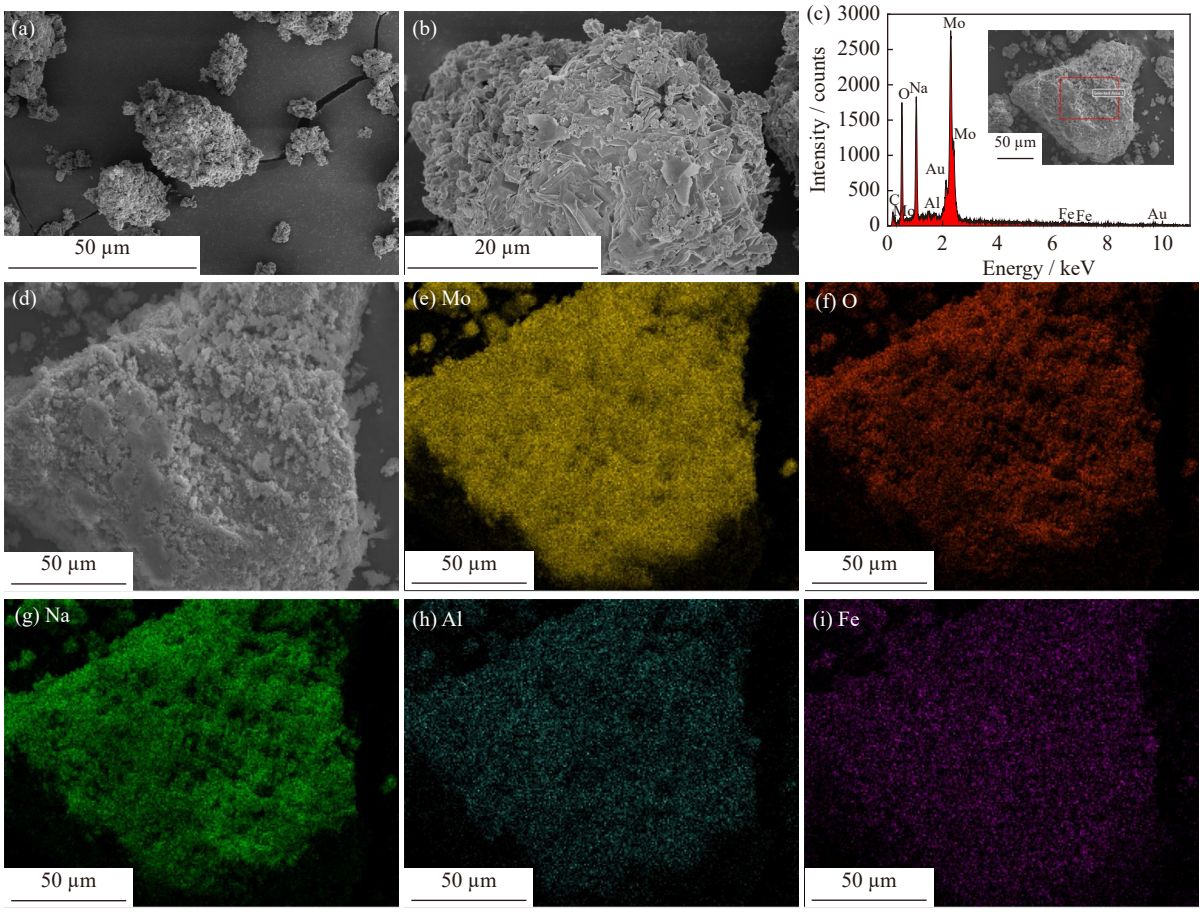

Fig. 12. Characterization of impure sodium molybdate: (a, b) SEM images; (c) EDS analysis; (d–i) surface scan analysis.

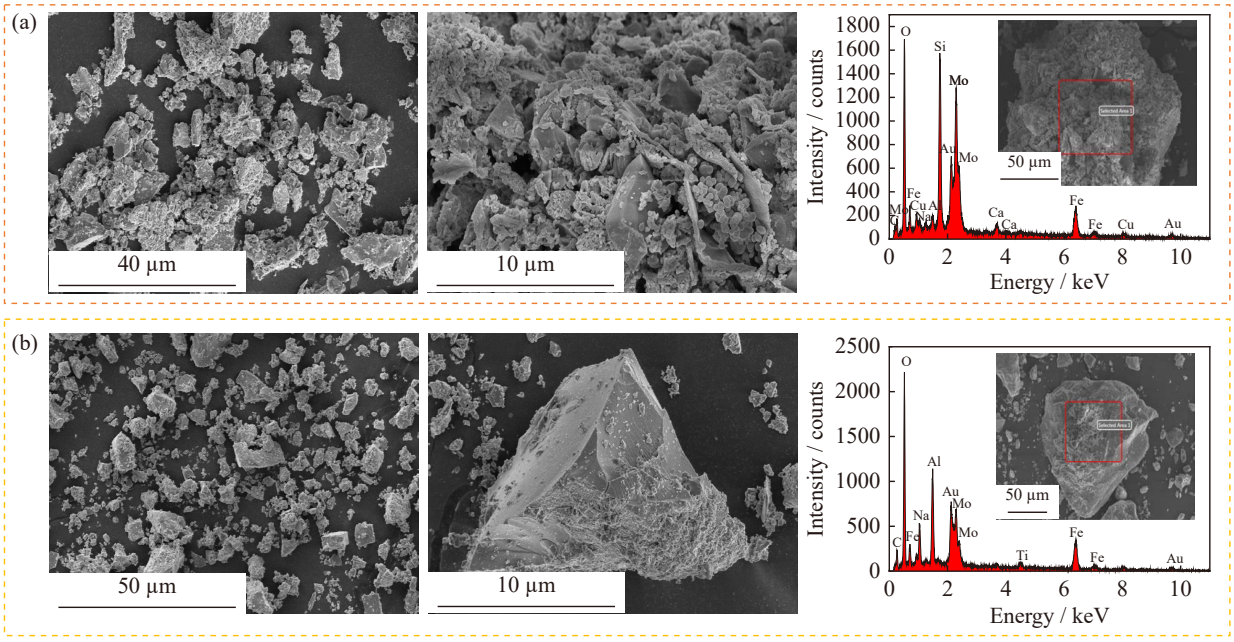

Fig. 13. SEM–EDS analysis results of (a) alkali-leached slag and (b) impurity slag.

data were fitted using Avantage, and the fitting results are shown in Fig. 15. In Fig. 15(a), the full spectrum shows all peaks of Mo, O, Na, and C. With the exception of C, all three elements (Mo, O, and Na) are derived from sodium molybdate, demonstrating its presence. Fig. 15(b) shows the spectrum of Mo 3d, from which the fitted peaks of Mo $3d_{3/2}$ and Mo $3d_{5/2}$ correspond to binding energies of 235.3 and 232.2 eV, respectively, indicating that the molybdenum in sodium molybdate is Mo^{6+}. Fig. 15(c) shows the spectrum of O 1s, which was fitted to two different peaks corresponding to oxygen vacancy (O_V) and lattice oxygen (O_L) [56]. In addition, the O_V and O_L correspond to binding energies of 531.9 and

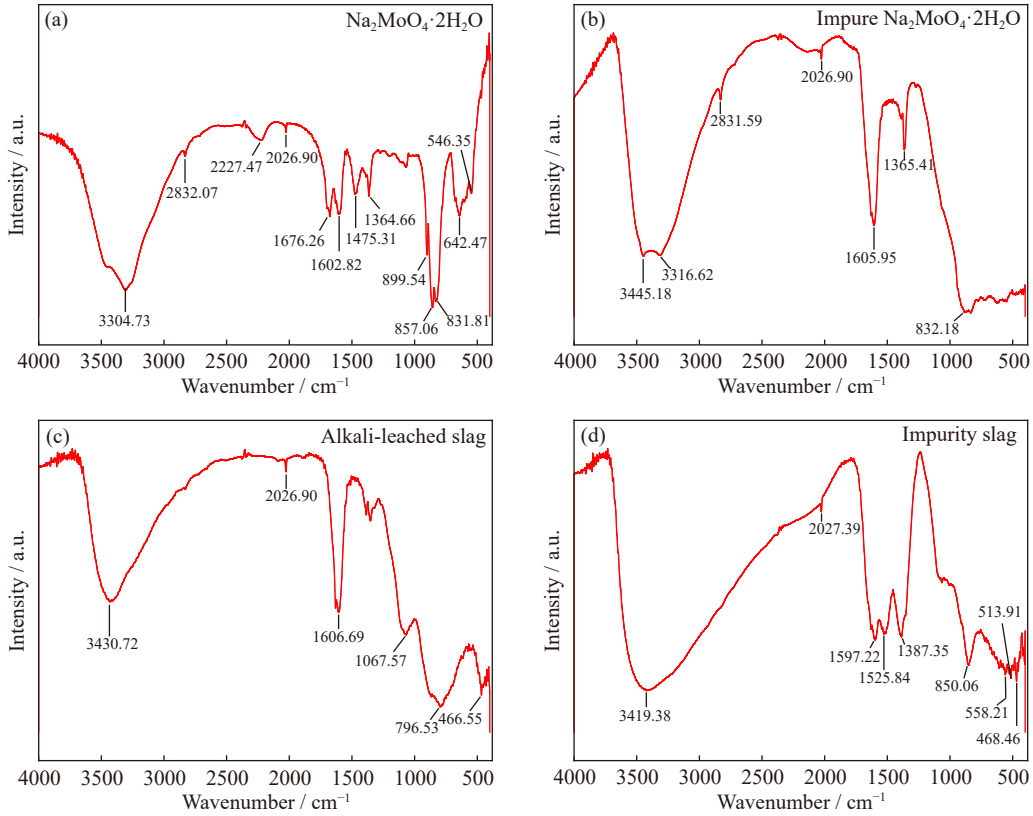

Fig. 14. FTIR spectra of (a) $Na_2MoO_4·2H_2O$, (b) impure $Na_2MoO_4·2H_2O$, (c) alkali-leached slag, and (d) impurity slag.

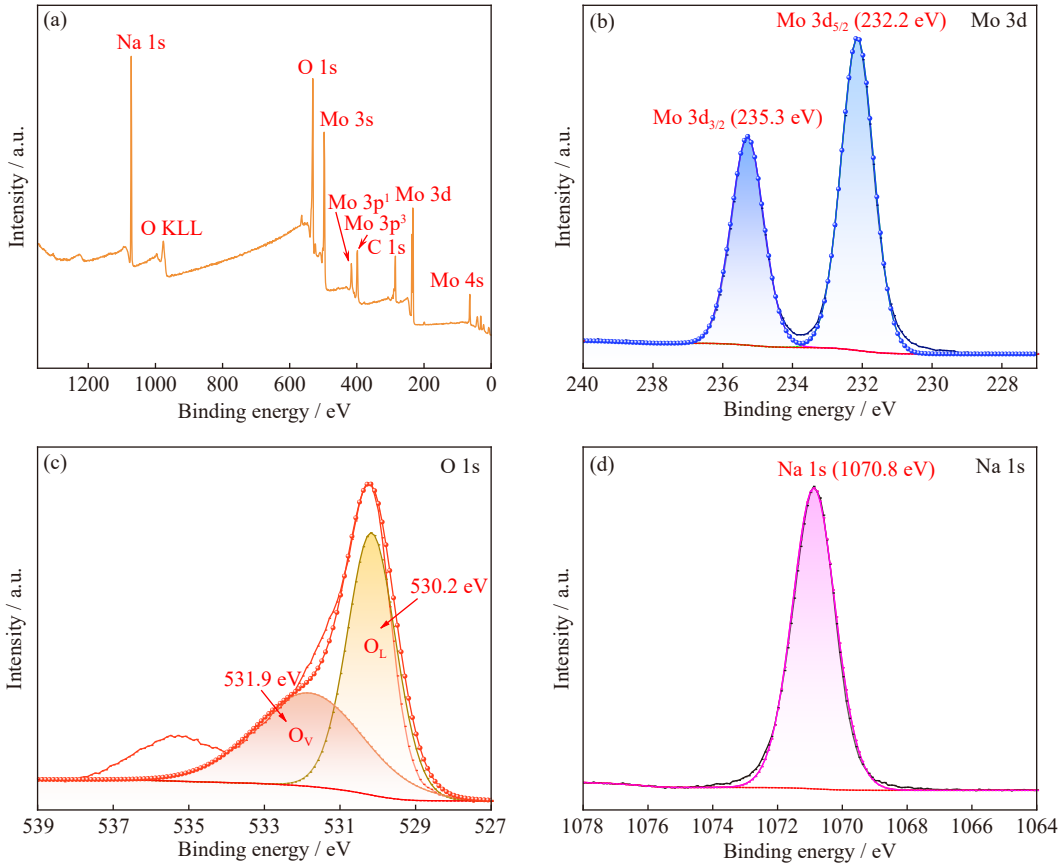

Fig. 15. XPS spectra of sodium molybdate: (a) full spectrum; (b) Mo 3d; (c) O 1s; (d) Na 1s.

530.2 eV, respectively. Only one sodium component (Na 1s) was fitted with a binding energy of 1070.8 eV. The XPS results show that the leached product is $Na_2MoO_4·2H_2O$, which is consistent with the predicted and other analytical results.

4. Conclusions

As an environmentally friendly and economical process, the present work introduces a microwave-based clean pyrometallurgical hydrometallurgical process for the production of sodium molybdate through three main processes: microwave roasting of the molybdenum concentrate, leaching with sodium hydroxide, and decontamination with sodium carbonate solution. The main findings are as follows.

(1) Thermodynamic analysis shows that oxidation roasting is thermodynamically feasible, demonstrating a dominant reaction of $MoS_2 + 3.5O_2(g) = MoO_3 + 2SO_2(g)$. The map of the dominant region of the Mo–O–S system reveals that the temperature increase favors the formation of MoO_3, while sufficient oxygen should be ensured to drive the MoS_2 reaction to completion.

(2) The optimal conditions for molybdenum recovery from molybdenum concentrate using microwave oxidation roasting of molybdenum concentrate included a roasting temperature of 700°C, a holding time of 110 min, and a power-to-mass ratio of 110 W/g.

(3) The optimal alkali leaching conditions were determined to be a NaOH concentration of 2.5 mol/L, a liquid-to-solid ratio of 2 mL/g, a leaching temperature of 60°C, and a terminated solution at pH 8. Under these conditions, the NaOH solution penetrates through the pores of the molybdenum calcine, completing the liquid–solid reaction and resulting the leaching rate of sodium molybdate of 96.24% and the content of 94.08wt%.

(4) Impurities such as iron and aluminum elements were efficiently eliminated via precipitation by adjusting the pH of the solution using sodium carbonate. The solution pH of 8 was found to remove impurities effectively based on the characterization of the sodium molybdate, alkali-leached slag, and impurity slag.

This study used microwave metallurgy to overcome the shortcomings of traditional metallurgical processes and generate high-purity sodium molybdate, harnessing the advantages of microwave metallurgy and providing new ideas for the future of metallurgy and sodium molybdate production.

Acknowledgements

This work was financially supported by the National Natural Science Foundation of China (No. 51964046).

Conflict of Interest

The authors have no competing interests to declare that are relevant to the content of this article.

References

[1] Q.S. Zhou, W.T. Yun, J.T, Xi, *et al*., Molybdenite–limestone oxidizing roasting followed by calcine leaching with ammonium carbonate solution, *Trans. Nonferrous Met. Soc. China*, 27(2017), No. 7, p. 1618.

[2] W. Yang, B.J. Deng, L.Q. Hou, *et al*., Sulfur-fixation strategy toward controllable synthesis of molybdenum-based/carbon nanosheets derived from petroleum asphalt, *Chem. Eng. J.*, 380(2020), art. No. 122552.

[3] O.P. Parenago, G.N. Kuz'mina, and T.A. Zaimovskaya, Sulfur-containing molybdenum compounds as high-performance lubricant additives (Review), *Pet. Chem.*, 57(2017), No. 8, p. 631.

[4] S. Kapri and S. Bhattacharyya, Molybdenum sulfide-reduced graphene oxide p–n heterojunction nanosheets with anchored oxygen generating manganese dioxide nanoparticles for enhanced photodynamic therapy, *Chem. Sci.*, 9(2018), No. 48, p. 8982.

[5] R.R. Mendel and F. Bittner, Cell biology of molybdenum, *Biochim. Biophys. Acta*, 1763(2006), No. 7, p. 621.

[6] B.N. Kaiser, K.L. Gridley, J. Ngaire Brady, T. Phillips, and S.D. Tyerman, The role of molybdenum in agricultural plant production, *Ann. Bot.*, 96(2005), No. 5, p. 745.

[7] S.C. Wang and L.Z. Wang, Recent progress of tungsten- and molybdenum-based semiconductor materials for solar-hydrogen production, *Tungsten*, 1(2019), No. 1, p. 19.

[8] W.W. Zhang, C.Y. Li, W.J. Wang, *et al*., Laminarin and sodium molybdate as efficient sustainable inhibitor for Q235 steel in sodium chloride solution, *Colloids Surf., A*, 637(2022), art. No. 128199.

[9] D.Q. Wang, M. Wu, J. Ming, and J.J. Shi, Inhibitive effect of sodium molybdate on corrosion behaviour of AA6061 aluminium alloy in simulated concrete pore solutions, *Constr. Build. Mater.*, 270(2021), art. No. 121463.

[10] Y. Zhou, Y. Zuo, and B. Lin, The compounded inhibition of sodium molybdate and benzotriazole on pitting corrosion of Q235 steel in NaCl+$NaHCO_3$ solution, *Mater. Chem. Phys.*, 192(2017), p. 86.

[11] O. Lopez-Garrity and G.S. Frankel, Corrosion inhibition of aluminum alloy 2024-T3 by sodium molybdate, *J. Electrochem. Soc.*, 161(2013), No. 3, p. C95.

[12] M.M. Heravi and M. Zakeri, Use of sodium molybdate dihydrate as an efficient heterogeneous catalyst for the synthesis of benzopyranopyrimidine derivatives, *Synth. React. Inorg. Met. Org. Nano Met. Chem.*, 43(2013), No. 2, p. 211.

[13] F. Torun, B. Hostins, P. De Schryver, N. Boon, and J. De Vrieze, Molybdate effectively controls sulphide production in a shrimp pond model, *Environ. Res.*, 203(2022), art. No. 111797.

[14] J. Bolitschek, S. Luidold, and M. O'Sullivan, A study of the impact of reduction conditions on molybdenum morphology, *Int. J. Refract. Met. Hard Mater.*, 71(2018), p. 325.

[15] L. Wang, G.H. Zhang, J.S. Wang, and K.C. Chou, Influences of different components on agglomeration behavior of MoS_2 during oxidation roasting process in air, *Metall. Mater. Trans. B*, 47(2016), No. 4, p. 2421.

[16] J.D. Lessard, D.G. Gribbin, and L.N. Shekhter, Recovery of rhenium from molybdenum and copper concentrates during the Looping Sulfide Oxidation process, *Int. J. Refract. Met. Hard Mater.*, 44(2014), p. 1.

[17] R. Jakhar, J.E. Yap, and R. Joshi, Microwave reduction of graphene oxide, *Carbon*, 170(2020), p. 277.

[18] J.P. Wang, T. Jiang, Y.J. Liu, and X.X. Xue, Influence of microwave treatment on grinding and dissociation characteristics of vanadium titano-magnetite, *Int. J. Miner. Metall. Mater.*, 26(2019), No. 2, p. 160.

[19] Y. He, J. Liu, J.H. Liu, C.L. Chen, and C.L. Zhuang, Carbothermal reduction characteristics of oxidized Mn ore through conventional heating and microwave heating, *Int. J. Miner. Metall. Mater.*, 28(2021), No. 2, p. 221.

[20] S. Das, A.K. Mukhopadhyay, S. Datta, and D. Basu, Prospects of microwave processing: An overview, *Bull. Mater. Sci.*, 31(2008), No. 7, p. 943.

[21] R.M. Anklekar, D.K. Agrawal, and R. Roy, Microwave sintering and mechanical properties of PM copper steel, *Powder Metall.*, 44(2001), No. 4, p. 355.
[22] J. Liu, C.H. Liu, Y. Hong, and L.B. Zhang, Basic study on microwave carbon-thermal reduction senarmontite (Sb_2O_3) to produce antimony: High-temperature dielectric properties and a microwave reduction mechanism, *Powder Technol.*, 389(2021), p. 482.
[23] V.Kvapilová, Evaluation of microwave drying effects on historical brickwork and modern building materials, *IOP Conf. Ser.: Mater. Sci. Eng.*, 867(2020), No. 1, art. No. 012026.
[24] M. Oghbaei and O. Mirzaee, Microwave versus conventional sintering: A review of fundamentals, advantages and applications, *J. Alloys Compd.*, 494(2010), No. 1-2, p. 175.
[25] G.Y. Zhu, Z.W. Peng, L. Yang, H.M. Tang, X.L. Fang, and M.J. Rao, Facile preparation of thermal insulation materials by microwave sintering of ferronickel slag and fly ash cenosphere, *Ceram. Int.*, 49(2023), No. 8, p. 11978.
[26] P. Parhi and P. Misra, Hydrometallurgical investigation routed through microwave (MW) assisted leaching and solvent extraction using ionic liquids for extraction and recovery of molybdenum from spent desulphurization catalyst, *Inorg. Chem. Commun.*, 149(2023), p. 110394.
[27] P.K. Parhi and P.K. Misra, Environmental friendly approach for selective extraction and recovery of molybdenum (Mo) from a sulphate mediated spent Ni–Mo/Al_2O_3 catalyst baked leach liquor, *J. Environ. Manage.*, 306(2022), art. No. 114474.
[28] S. Kan, K. Benzeşik, Ö.C. Odabaş, and O. Yücel, Investigation of molybdenite concentrate roasting in chamber and rotary furnaces, *Min. Metall. Explor.*, 38(2021), No. 3, p. 1597.
[29] Y.L. Jiang, B.G. Liu, P. Liu, J.H. Peng, L.B. Zhang, Dielectric characterization and microwave roasting of molybdenite concentrates at 915 MHz frequency, *J. Harbin Inst. Technol. (New Series)*, 26(2019), No. 3, p. 58.
[30] M. Pervaiz, A. Munawar, S. Hussain, *et al*., A green approach for extraction of ammonium molybdate from molybdenite using indigenous resources, *Pol. J. Environ. Stud.*, 30(2021), No. 2, p. 1771.
[31] M.P. Zhang, C.H. Liu, X.J. Zhu, *et al*., Preparation of ammonium molybdate by oxidation roasting of molybdenum concentrate: A comparison of microwave roasting and conventional roasting, *Chem. Eng. Process.: Process. Intensif.*, 167(2021), art. No. 108550.
[32] M.D. Lane, J.L. Bishop, M.D. Dyar, *et al*., Mid-infrared emission spectroscopy and visible/near-infrared reflectance spectroscopy of Fe-sulfate minerals, *Am. Mineral.*, 100(2015), No. 1, p. 66.
[33] L. Wang, G.H. Zhang, J. Dang, and K.C. Chou, Oxidation roasting of molybdenite concentrate, *Trans. Nonferrous Met. Soc. China*, 25(2015), No. 12, p. 4167.
[34] H. Sun, G.H. Li, Q.Z. Bu, *et al*., Features and mechanisms of self-sintering of molybdenite during oxidative roasting, *Trans. Nonferrous Met. Soc. China*, 32(2022), No. 1, p. 307.
[35] C. Kansomket, P. Laokhen, T. Yingnakorn, T. Patcharawit, and S. Khumkoa, Extraction of molybdenum from a spent HDS catalyst using alkali leaching reagent, *J. Met. Mater. Miner.*, 32(2022), No. 2, p. 88.
[36] C. Wang, Y.F. Guo, S. Wang, *et al*., Characteristics of the reduction behavior of zinc ferrite and ammonia leaching after roasting, *Int. J. Miner. Metall. Mater.*, 27(2020), No. 1, p. 26.
[37] Y.I. Nam, S.Y. Seo, Y.C. Kang, M.J. Kim, G. Senanayake, and T. Tran, Purification of molybdenum trioxide calcine by selective leaching of copper with HCl–NH_4Cl, *Hydrometallurgy*, 109(2011), No. 1-2, p. 9.
[38] H. Sun, J.J. Yu, G.H. Li, *et al*., Co-volatilizing-water leaching process for efficient utilization of rhenium-bearing molybdenite concentrate, *Hydrometallurgy*, 192(2020), art. No. 105284.
[39] J.H. Chen, D. Tang, S.P. Zhong, W. Zhong, and B.Z. Li, The influence of micro-cracks on copper extraction by bioleaching, *Hydrometallurgy*, 191(2020), art. No. 105243.
[40] L.P. Jia, Z.W. Zhao, X.H. Liu, and L.H. He, Recovery of valuable metals from molybdenum-removal sludge by reverse sulfurization leaching, *Hydrometallurgy*, 193(2020), art. No. 105323.
[41] Y.B. Li, Q.H. Xiao, Z.M. Li, and Gerson A, Enhanced leaching of Mo by mechanically co-grinding and activating MoS_2 with $NaClO_3$ as an oxidizing additive, *Hydrometallurgy*, 203(2021), art. No. 105625.
[42] S. Ali, Y. Iqbal, I. Khan, *et al*., Hydrometallurgical leaching and kinetic modeling of low-grade manganese ore with banana peel in sulfuric acid, *Int. J. Miner. Metall. Mater.*, 28(2021), No. 2, p. 193.
[43] J. Liu, Z.F. Qiu, J. Yang, L.M. Cao, and W. Zhang, Recovery of Mo and Ni from spent acrylonitrile catalysts using an oxidation leaching–chemical precipitation technique, *Hydrometallurgy*, 164(2016), p. 64.
[44] Z.X. Liu, L. Sun, J. Hu, *et al*., Selective extraction of molybdenum from copper concentrate by air oxidation in alkaline solution, *Hydrometallurgy*, 169(2017), p. 9.
[45] P. Wang, Y.J. Pan, X. Sun, and Y.Q. Zhang, Leaching molybdenum from a low-grade roasted molybdenite concentrate, *SN Appl. Sci.*, 1(2019), No. 4, art. No. 311.
[46] M. Vosough, G.R. Khayati, and S. Sharafi, Ammonia leaching of MoO_3 concentrate: Finding the reaction mechanism and kinetics analysis, *Chem. Pap.*, 76(2022), No. 5, p. 3227.
[47] Z.P. Zhao, M. Guo, and M. Zhang, Extraction of molybdenum and vanadium from the spent diesel exhaust catalyst by ammonia leaching method, *J. Hazard. Mater.*, 286(2015), p. 402.
[48] Y. Liu, Y.F. Zhang, F.F. Chen, and Y. Zhang, The alkaline leaching of molybdenite flotation tailings associated with galena, *Hydrometallurgy*, 129-130(2012), p. 30.
[49] Y. Guo, H.Y. Li, Y.H. Yuan, *et al*., Microemulsion leaching of vanadium from sodium-roasted vanadium slag by fusion of leaching and extraction processes, *Int. J. Miner. Metall. Mater.*, 28(2021), No. 6, p. 974.
[50] G.J. Olson and T.R. Clark, Bioleaching of molybdenite, *Hydrometallurgy*, 93(2008), No. 1-2, p. 10.
[51] Y.F. Fu, Q.G. Xiao, Y.Y. Gao, P.G. Ning, H.B. Xu, and Y. Zhang, Pressure aqueous oxidation of molybdenite concentrate with oxygen, *Hydrometallurgy*, 174(2017), p. 131.
[52] J.P. Wang, Y.M. Zhang, J. Huang, and T. Liu, Synergistic effect of microwave irradiation and CaF_2 on vanadium leaching, *Int. J. Miner. Metall. Mater.*, 24(2017), No. 2, p. 156.
[53] S.A. Kapole, B.A. Bhanvase, D.V. Pinjari, *et al*., Investigation of corrosion inhibition performance of ultrasonically prepared sodium zinc molybdate nanopigment in two-pack epoxy-polyamide coating, *Compos. Interfaces*, 21(2014), No. 9, p. 833.
[54] S. Nakagaki, A. Bail, V.C. dos Santos, *et al*., Use of anhydrous sodium molybdate as an efficient heterogeneous catalyst for soybean oil methanolysis, *Appl. Catal. A*, 351(2008), No. 2, p. 267.
[55] Y. Mochizuki, J. Bud, J.Q. Liu, M. Takahashi, and N. Tsubouchi, Adsorption of phosphate from aqueous using iron hydroxides prepared by various methods, *J. Environ. Chem. Eng.*, 9(2021), No. 1, art. No. 104645.
[56] S.Q. Wang, J. Xie, J.D. Hu, H.Y. Qin, and Y.L. Cao, Fe-doped α-MoO_3 nanoarrays: Facile solid-state synthesis and excellent xylene-sensing performance, *Appl. Surf. Sci.*, 512(2020), art. No. 145722.